MEAN AND TURBULENT STRUCTURE OF A BAROCLINIC MARINE BOUNDARY LAYER DURING THE 28 JANUARY 1986 COLD-AIR OUTBREAK (GALE 86)

ROBERT J. WAYLAND* and SETHU RAMAN

North Carolina State University, Raleigh, North Carolina 27612, U.S.A.

(Received in final form 21 March, 1989)

Abstract. Aircraft (NCAR Electra), ship (R/V Cape Hatteras), buoy (NCSU Buoy 2) and satellite (NOAA-7 and 9) measurements have been used to observe the structure of the Marine Boundary Layer (MBL) offshore of Wilmington, North Carolina, during the intense cold-air outbreak of 28 January, 1986, as part of the Genesis of Atlantic Lows Experiment (GALE). Air mass modification processes, driven primarily by the surface turbulent latent and sensible heat fluxes, caused the overlying air mass to warm and moisten as it advected over the warmer waters of the eastern United States continental shelf. Maximum observed total (latent + sensible) heat flux was 1045 W/m^2 (at a height of 49 m) over the core of the Gulf Stream. Heat flux values decreased both east and west of this region, primarily in response to changes in the air-sea temperature difference.

MBL height increased steadily in the offshore direction in response to increasing convection. The turbulent structure showed a buoyancy-dominated MBL between $0.1z/h$ and $0.8z/h$; whereas shear was important above and below this level, vertical transport of kinetic energy (KE) was dominant as a source term only above $0.8z/h$. The normalized turbulent kinetic energy (TKE) budgets observed at different offshore locations showed general agreement at different flight levels. Thus the findings support the validity of the similarity relations under intense convective conditions.

1. Introduction

The amount of heat and moisture available to the atmosphere from the sea surface is very large in the regions surrounding eastern continental margins. The conditions are optimized geographically along the east coast of the United States, and seasonally during the winter months when the water-land temperature contrast is a maximum. The geography is unique in that there is a cold continent bounded by the relatively warmer shelf/slope water, which is again bounded by the consistently warmer Gulf Stream waters. The slightly cooler Sargasso Sea region borders the Gulf Stream in the east (Figure 1). Each of these underlying surfaces causes a different response in boundary layer growth and its structure due to changes in the stability parameters and surface roughness. The Marine Boundary Layer (MBL) thus becomes strongly baroclinic.

Due to the large fluxes of momentum, heat and moisture in these regions, numerous atmospheric events such as low pressure systems and coastal fronts develop and strengthen in these waters (Bunker and Worthington, 1976). Colucci

* Present affiliation: Science Applications International Corporation, Raleigh, North Carolina 27606.

Boundary-Layer Meteorology **48**: 227–254, 1989.

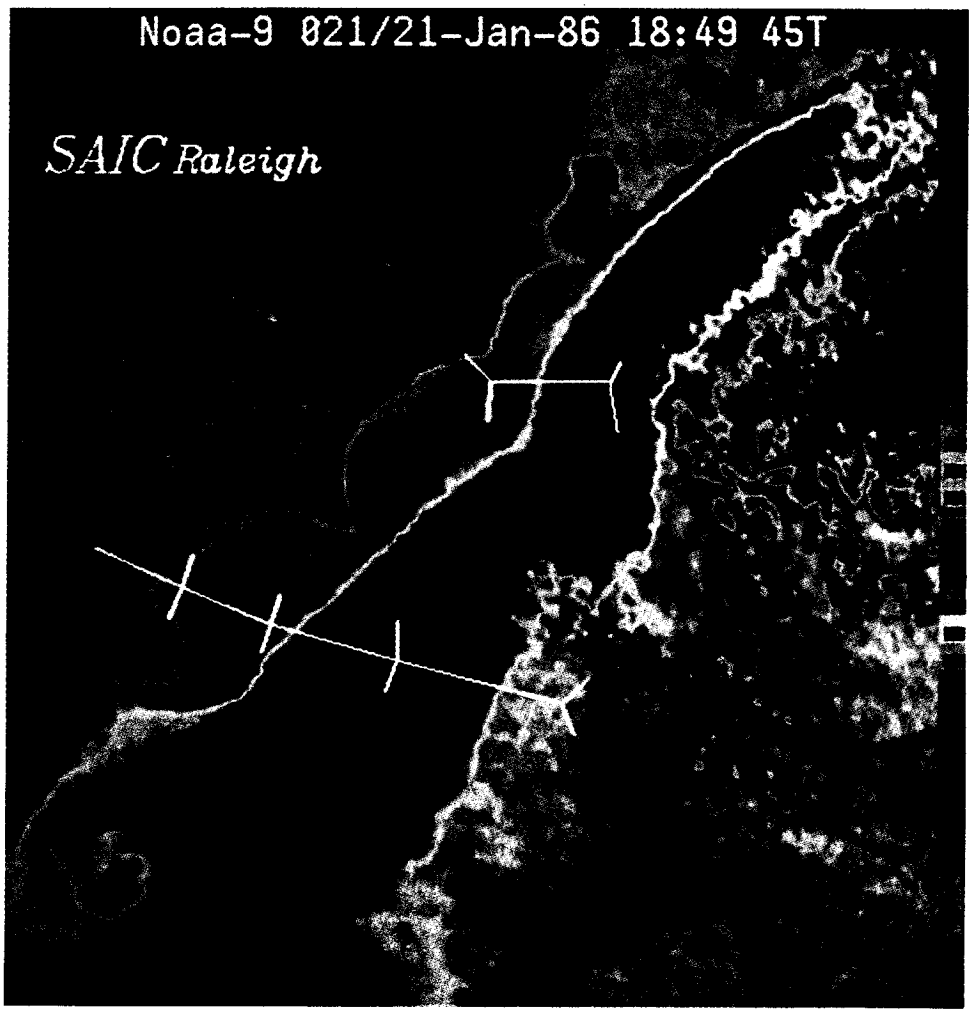

Fig. 1. NOAA-9 AVHRR satellite image (channels 4 and 5, atmospherically corrected) from 21 January, 1986 (approximately one week prior to aircraft mission) showing the NCAR Electra and King Air (not discussed here) flight tracks for the 28 January, 1986 mission. The distinct oceanic features (inner shelf, shelf break, Gulf Stream Core and Eastern Gulf Stream Wall) can easily be seen.

(1976), Hayden (1981) and Hayden and Smith (1982) have presented statistical analyses showing the persistence of cyclonic features offshore of the mid-Atlantic coast and in approximate orientation with the Gulf Stream axis. However, in terms of energy exchange, one of the most dynamic of these events is the cold air outbreak, which occurs when a cold, dry continental air mass moves out over the warmer ocean. About 15–20 cold-air outbreak events affect the mid-Atlantic region annually, while approximately five of these systems can be classified as intense (air temperature $< 0\,^{\circ}C$) events (Grossman, 1988). The duration of these systems is generally on the order of one to two days. Fernandez-Partegas and Mooers (1975) have investigated cold air-air outbreaks in the Gulf of Mexico

region and found that they occur at 3–10 day intervals from October through April. Huh *et al.* (1984) found these events in the Gulf of Mexico to be highly dependent on the horizontal air-sea temperature and humidity gradients and mean wind speed, all of which change rapidly across the inner continental shelf.

Cold-air outbreaks cause changes in both the overlying air mass and the underlying ocean surface layer and have been studied in recent years (Nowlin and Parker, 1974; Lenschow and Agee, 1976; Lenschow *et al.*, 1980; Chou and Atlas, 1982; Huh *et al.*, 1984; Chou *et al.*, 1986; SethuRaman *et al.*, 1986). In the past ten years, two major field programs have been conducted to study the effects of cold-air outbreaks on the air mass modification processes. The Air-Mass Transformation Experiment (AMTEX) was conducted during February 1974 and 1975 over the East China Sea in the vicinity of the warm Kuroshio current (Lenschow and Agee, 1976; Murty, 1976; Lenshow *et al.*, 1980). In January 1983, the Mesoscale Air-Sea Exchange (MASEX) experiment was conducted offshore of the eastern United States coast in close proximity to the Gulf Stream (Chou and Atlas, 1982; Chou *et al.*, 1986).

Recently, the Genesis of Atlantic Lows Experiment (GALE) was conducted in the mid-Atlantic coastal region of the United States. The GALE project, carried out between January 15–March 15, 1986, was one of the largest weather experiments conducted in the United States. Aircraft, radar, sounding systems, satellites, ships and buoys were utilized throughout GALE to monitor changes in atmospheric/oceanic conditions. The main purpose of this experiment was to determine the processes involved in the development of extratropical cyclones offshore of the Carolinas. The objective was also to study several other mesoscale phenomena such as cold-air damming, cold-air outbreaks, and rain bands, and investigate their relative contributions to offshore/onshore cyclogenesis events. Design of the experiment is discussed by Dirks *et al.* (1988) and a description of the Planetary Boundary Layer (PBL) observation systems is given by Raman and Riordan (1988).

The purpose of this paper is to discuss a portion of one of the thirteen intensive observation periods (IOP's), covering the intense cold-air outbreak of 28 January, 1986 (IOP #2). Data collected using the National Center for Atmospheric Research (NCAR) Electra and the research vessel R/V Cape Hatteras are utilized to study the mean and turbulent structure of the atmosphere, while Advanced Very High Resolution Radiometer (AVHRR) data from the NOAA-7 and NOAA-9 polar-orbitting satellites are used to analyze oceanic surface temperature features. The satellite data have been atmospherically corrected using input data from channels 4 and 5 and mapped on a 4 by 4 km grid for both satellites. Figure 2 illustrates the flight and cruise tracks of the NCAR Electra and R/V Cape Hatteras and the position of NCSU Buoy 2. The cruise plan of the R/V Cape Hatteras also details the location and the launch sequence of the minisonde soundings.

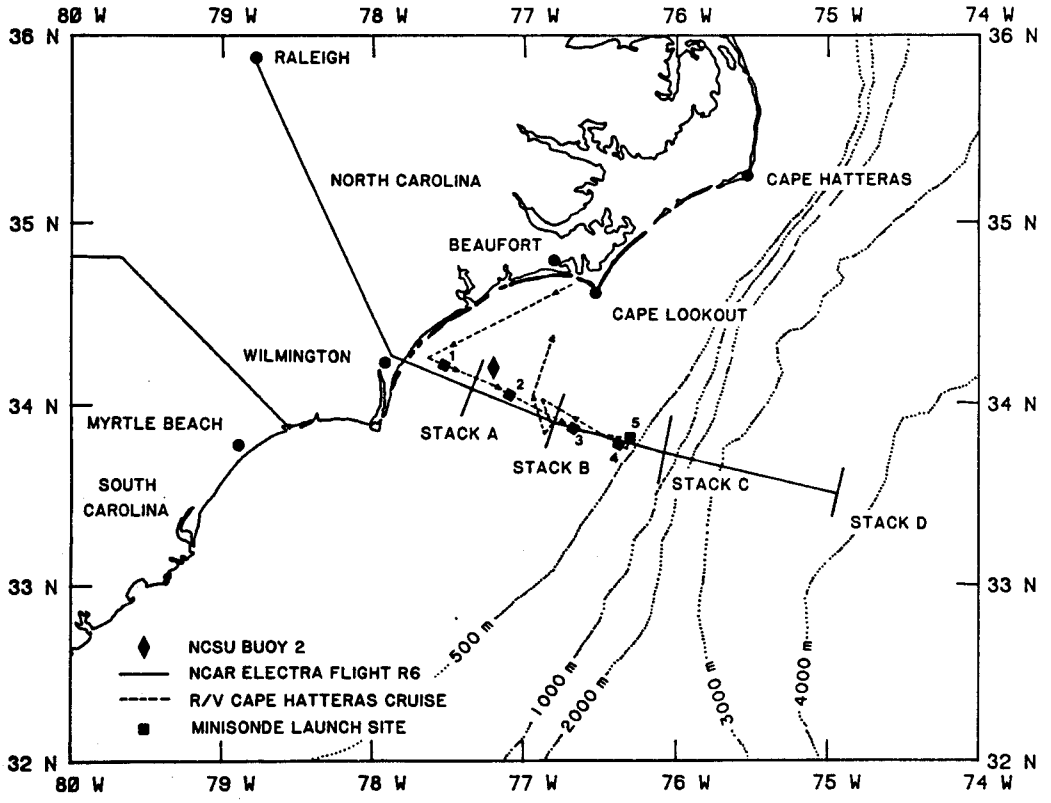

Fig. 2. Flight plan for the NCAR Electra (solid line) for mission R6 on 28 January, 1986. Research stations A–D were flown approximately crosswind, with transit between these regions made approximately along the mean wind. Cruise track for the NCSU research vessel R/V Cape Hatteras (dashed line) on 28–29 January, 1986. The locations of the three-hourly minisonde launches (■) are given, beginning with station 1 at 1115 GMT.

2. Synoptic Conditions

A detailed analysis of the synoptic conditions on 28 January, 1986 is given by Uccellini *et al.* (1986). A strong cold front moved through the GALE research area on the evening of 27 January, resulting in extremely cold, dry air filtering into the southeastern portion of the United States late on 27 January and into 28 January. A summary of synoptic conditions on 28 January, 1986 is shown in Figure 3. Cold air advection was associated with a strong high pressure ridge along the Texas Gulf Coast pushing eastward, and a rapidly intensifying extratropical storm moving offshore towards the northeast. The combined circulations of these two systems acted to funnel the cold air into the GALE research area.

The 0000 GMT and 0600 GMT upper air soundings at Cape Hatteras showed strong cold air advection (as evidenced by the backing of the wind with height) at this coastal location, just north of the planned aircraft mission region. At the time of aircraft departure (1500 GMT) from the Raleigh-Durham (RDU) airport, surface temperatures were sub-zero throughout the GALE research region over

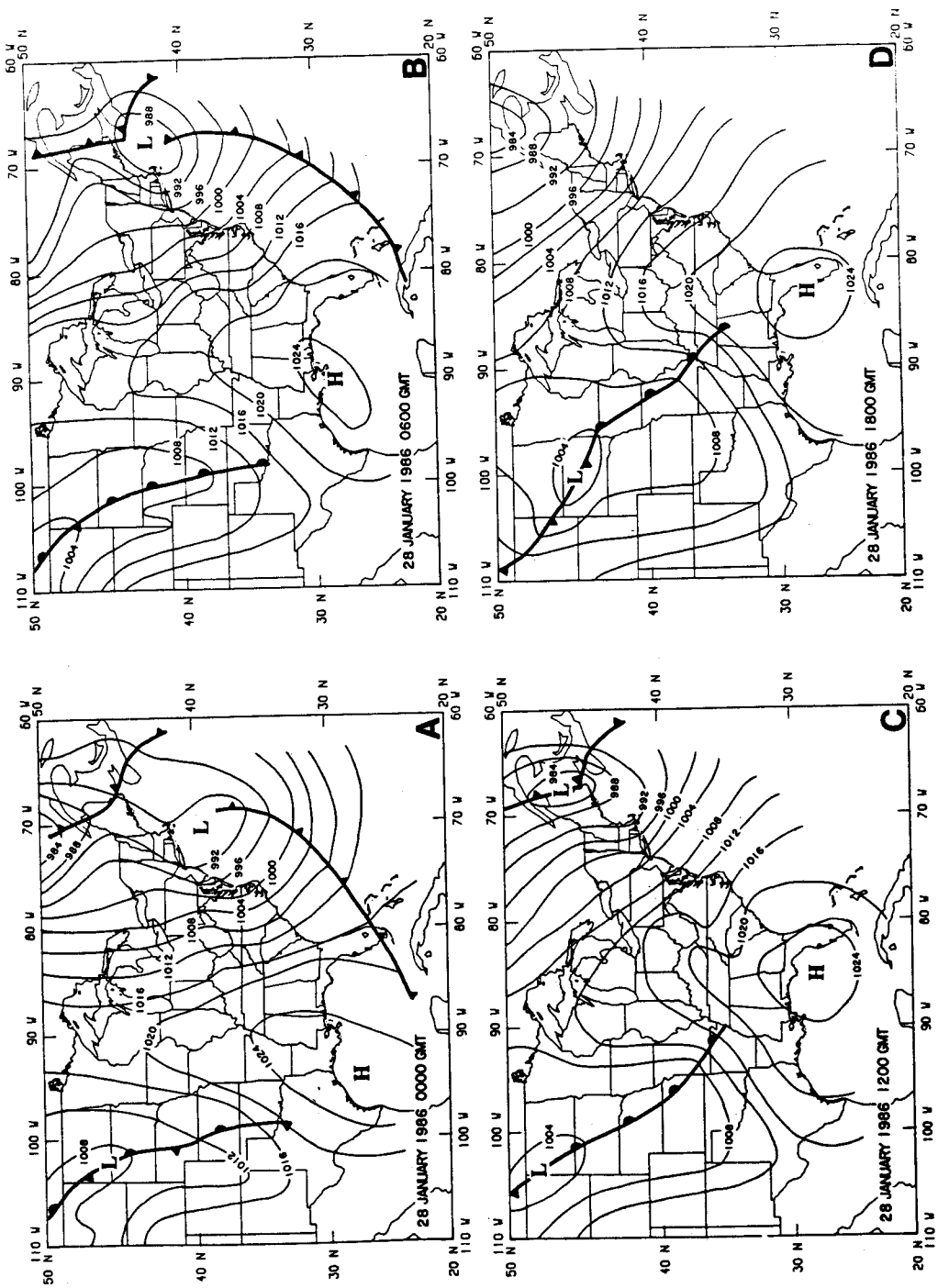

Fig. 3. Summary of synoptic conditions surrounding the intense cold air outbreak: (A) 0000 GMT 28 January, 1986, (B) 0600 GMT, (C) 1200 GMT, (D) 1800 GMT.

land. The winds were predominantly from a west-northwesterly direction. Offshore of Wilmington, North Carolina, the cold-air outbreak created air-water temperature contrasts as high as 24.4 °C. Also, soundings at both Wilmington and Cape Hatteras, North Carolina, showed that the cold air advection had subsided considerably over the region by 1800 GMT, indicating that the cold air was well entrenched over the flight area during the observation period.

3. Methodology

The initial flight and cruise plans were designed to allow a reasonable reconstruction of the mean and turbulent structure of the Marine Boundary Layer offshore of Wilmington, North Carolina. The NCAR Electra departed RDU, proceeding southeast enroute to Wilmington, at 1500 GMT. Upon arrival at the coast (approximately near Wilmington) the aircraft completed a ramp descent sounding to determine boundary layer height and began a 284 km offshore transect (heading 135 deg, essentially alongwind) enroute to the first research station (the most offshore point). During this offshore transit, the aircraft track was designed to maintain altitude just below the cloud base. As the aircraft traversed the area, the onboard, downward-looking infrared radiometer data were analyzed in real-time to position the locations of the four crosswind research stations to be investigated on the inbound phase of the mission.

In general, the weather conditions degraded with increasing distance offshore. The eastern region of North Carolina was clear and the inner shelf area (<30 km offshore) remained partially clear. This can be seen in the GOES visible image presented in Figure 4. The first evidence of sea smoke on the water surface appeared approximately 10–15 km downwind of Wilmington. With increasing distance offshore and increasing proximity to the Gulf Stream front, the overhead stratocumulus deck thickened, becoming totally overcast near the western edge of the Gulf Stream. Coincident with the overcast conditions, there was an increase in the number and intensity of steam devils and sea smoke. Over the core of the Gulf Stream, the cloud base began to decrease rapidly and the filament structures evident in the sea smoke connected the ocean surface to the cloud bases. Upon arrival at the eastern most extent of the flight track, ascent to approximately 2400 m was made, revealing cumulus congestus and frequent regions of penetrative convective cells. These cells were clearly evident during the cloud top flight made at research station D. See Figures 2 and 5 for locations of Stations A, B, C and D. The presence of similar penetrative thermals was also pointed out by Chou *et al.* (1986) in their analysis of the upper level flight legs of the MASEX data.

Figure 5 is a schematic of the flight levels with respect to the varying sea surface temperature (SST) structure. A stack is composed of multiple levels (each at a different altitude) flown along a constant heading at a relatively constant airspeed. In the case of the NCAR Electra, levels were flown both

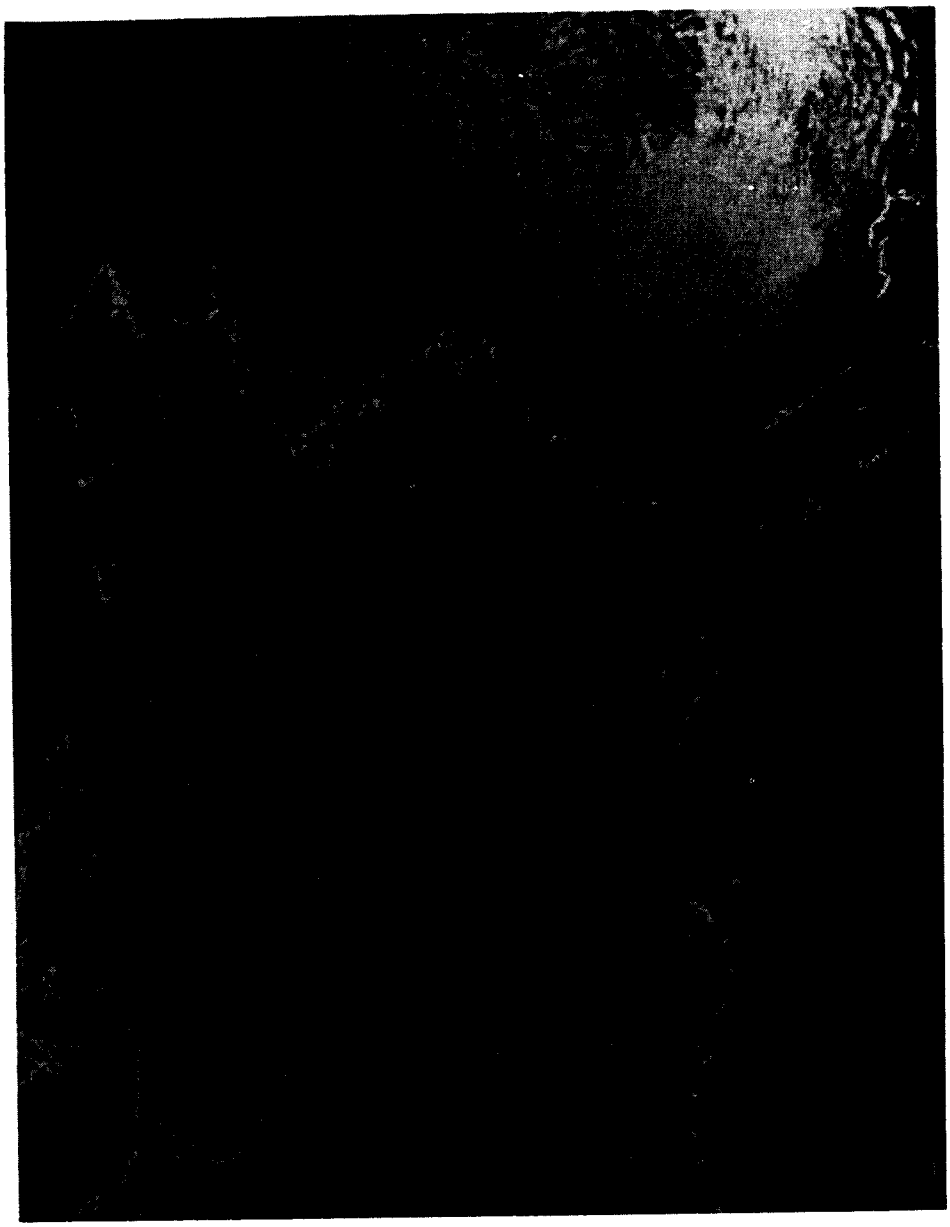

Fig. 4. GOES-6 4 km visible satellite image 1800 GMT 28 January, 1986 (from Mercer and Kreitzberg, 1986).

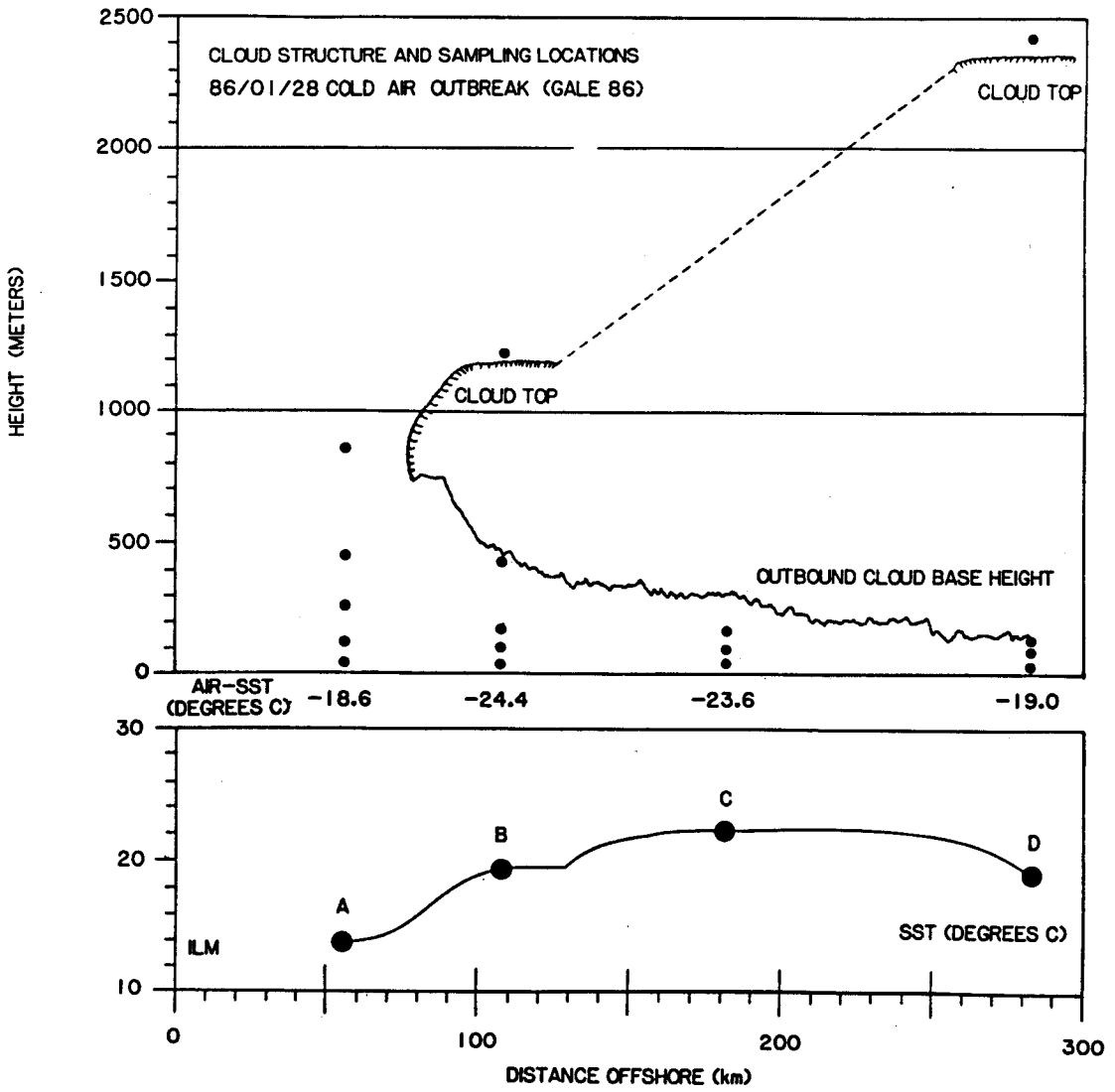

Fig. 5. Schematic diagram showing the change in sea surface temperature (SST) at each of the four crosswind research stations and the general cloud structure sampled at each location. The large dots indicate the research locations, while the smaller dots indicate the levels for each crosswind flight level.

below and above the cloud base altitude at approximately 100 m/s along the headings 30°–210° True. The first stack, research point D (33° 31.5′ N, 75° 02.6′ W), was located near the eastern wall region of the Gulf Stream, 284 km offshore from Wilmington. A ramp ascent was made here to determine boundary layer height. From onboard analysis of the potential temperature and specific humidity profiles, the mixed-layer height was fixed at approximately 2300 m. On descent, a four-level (48, 122, 157 and 2424 m) crosswind stack was flown, with the Electra spending approximately 8 min (at a constant heading) at each flight level. The lowest three levels were flown in the sub-cloud region, while the uppermost leg was just above cloud tops. However, due to the large number of

penetrative convective cells in this region, the aircraft was at times in the clouds during this above-cloud transit. Flight from research station D to point C was made along a heading of 235 deg at 48 m Above Sea Level (ASL).

At station C (33° 43.8′ N, 76° 02.6′ W), located near the core of the Gulf Stream axis, a three-level (48, 107 and 173 m) crosswind stack was flown. All three levels were in the sub-cloud region due to fuel and time requirements for attaining cloud-top altitude at this location. However, a minisonde potential temperature sounding from the R/V Cape Hatteras located just to the west of station C was used to fix the boundary-layer height at 1400 m, based on the height of the capping inversion. Travel from station C across the Gulf Stream front into the shelf-break region at station B was made at 41 m.

A five-level (32, 99, 175, 445 and 1215 m) crosswind stack was flown at station B (33° 54.0′ N, 76° 47.2′ W) followed by a ramp descent sounding. The resulting profiles fixed the boundary-layer height at station B near 1100 m. Transit from station B to the inner shelf region at station A was made at 40 m, heading 300 deg. Upon approach to station A, clear skies to the west were quite evident along with a decrease in turbulence in the atmospheric boundary layer.

Station A (34° 04.8′ N, 77° 19.0′ W) was located in the cool shelf waters of the inner shelf region, only 55 km downwind from the coast near Wilmington. This was a region of relatively cooler water (14.1 °C), well out of the influence of the warmer Gulf Stream and its associated circulation features (e.g., warm core rings and filaments). A five-level (38, 111, 268, 444 and 868 m) crosswind stack was completed here, after which a ramp ascent to 3049 m was made.

In support of the planned/anticipated aircraft mission(s), the R/V Cape Hatteras steamed from its home port in Beaufort, North Carolina, at 0200 GMT 28 January, 1986. The vessel steamed parallel to the coast for approximately 8 h prior to turning with the wind around 1000 GMT. The resulting cruise track essentially paralleled the NCAR Electra flight track (out to the Gulf Stream region). In fact, the R/V Cape Hatteras was sighted by the Electra during a low-level flight between stations C and B. At 1115 GMT, 3-hrly minisonde launches began from the R/V Cape Hatteras. Table I gives a description of each

TABLE I

Description and location of 28 January, 1986 R/V Cape Hatteras minisonde launches made in support of NCAR Electra mission R6.

Sounding number	Date	Latitude (degrees)	Longitude (degrees)	Time (GMT)
1	86/01/28	34° 12.4′ N	77° 29.9′ W	1115
2	86/01/28	34° 03.4′ N	77° 06.5′ W	1415
3	86/01/28	33° 52.2′ N	76° 41.7′ W	1715
4	86/01/28	33° 46.6′ N	76° 22.4′ W	2015
5	86/01/28	33° 48.7′ N	76° 18.3′ W	2315

of the five minisonde launches made during the cruise. This information provided valuable temporal and spatial coverage of the evolution and growth of the MBL offshore of Wilmington, North Carolina.

The final piece of information utilized is shown in Figure 6, which is a NOAA-7, AVHRR polar-orbiting satellite image (channels 4 and 5, atmospherically corrected) taken at 2110 GMT, which delineates the discrete oceanographic features in the region traversed by the Electra. Unfortunately, the two easternmost research stations were completely overcast due to stratocumulus, cumulus congestus and sea smoke and thus it was impossible to obtain a clear SST image from the satellite. However, the two inshore locations (as seen in Figure 6) are well outside the cloud shield and show the complex oceanic thermal structure which greatly affects the air mass modification process. Notice the 4 to

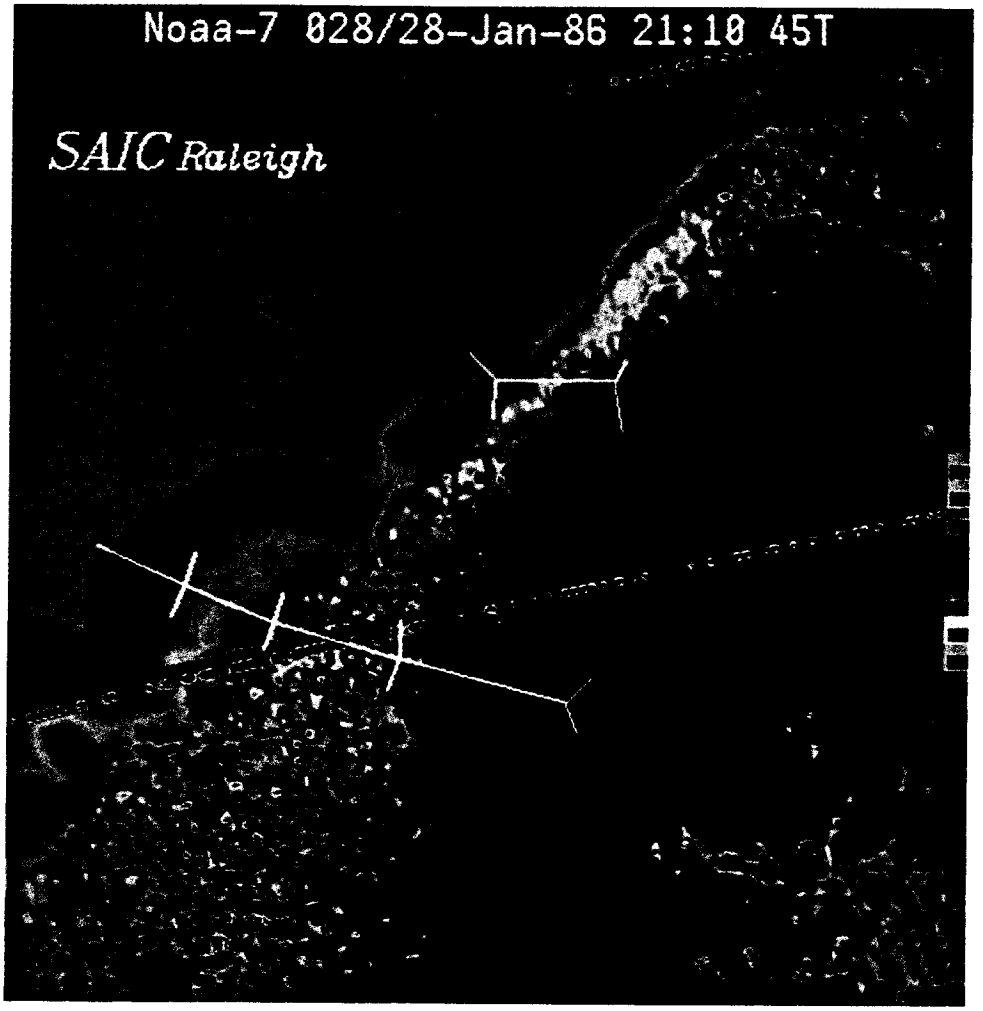

Fig. 6. NOAA-7 AVHRR satellite image (channels 4 and 5, atmospherically corrected) from 2110 GMT 28 January, 1986 showing the NCAR Electra (and King Air) flight track and crosswind research locations. The cloud cover in the vicinity of the Gulf Stream is also easily visible.

5 °C decrease in SST at the inner shelf (A) location for 28 January, 1986 as compared to the earlier image on 21 January, 1986 (Figure 1).

4. Observations and Analysis

The NCAR Electra research aircraft collected data used in analyzing both the mean and turbulent structure of the MBL. The Aircraft Data System (ADS) is an onboard computer specifically designed for real-time processing/display and archiving of all meteorological data collected during flight. The central element is the Litton LTN-51 inertial navigation system (INS), which outputs the aircraft latitude and longitude at 1-s intervals. The wind components are then derived from the various INS output parameters. The temperature used in both the mean and turbulent analyses was measured using the boom-mounted Rosemount Model 102 fast-response temperature sensor. The slow-response humidity data, used to calibrate the fast-response, high-resolution Lyman-alpha (hydrogen absorption) sensor, was obtained from the EG & G Model 137 dewpoint hygrometer. The SST temperature was collected using a downward-looking, narrow bandwidth narrow field of view (2°) Barnes Engineering Model PRT-5 precision radiation thermometer (Miller and Friesen, 1985).

The data were then pre-processed at NCAR and made available to the GALE Data Center for distribution. The data were separated into flight legs at near constant heading and altitude to avoid any contamination due to aircraft turns, climbs or descents. The exceptions to this procedure involved the previously mentioned ramp soundings made by the Electra where descent/ascent was made along a constant heading, attempting to profile the boundary layer during this particular maneuver.

In the data analysis, the high-rate data, sampled at 20 samples per second (sps), were used in all turbulent flux calculations and to generate the mean data values for each flight leg. The only slow rate data (sampled at 1 sps) used were the position information output from the INS, the SST output from the infrared sensor and the specific humidity, which was used to calibrate the Lyman-alpha sensor. Turbulent fluxes were calculated using simple statistics involving the covariance and correlation between the two variables of interest. Energy dissipation was estimated using the vertical velocity (w-component) spectra in conjunction with the $-5/3$ power law of Kolmogorov.

5. Discussion of Results

5.1. Mean Structure

Vertical variation of the mean values of wind speed, wind direction, potential temperature and specific humidity at different locations offshore are shown in Figure 7. The dashed lines refer to regions where no detailed data were collected, and are drawn to connect the regions where crosswind stack levels were flown.

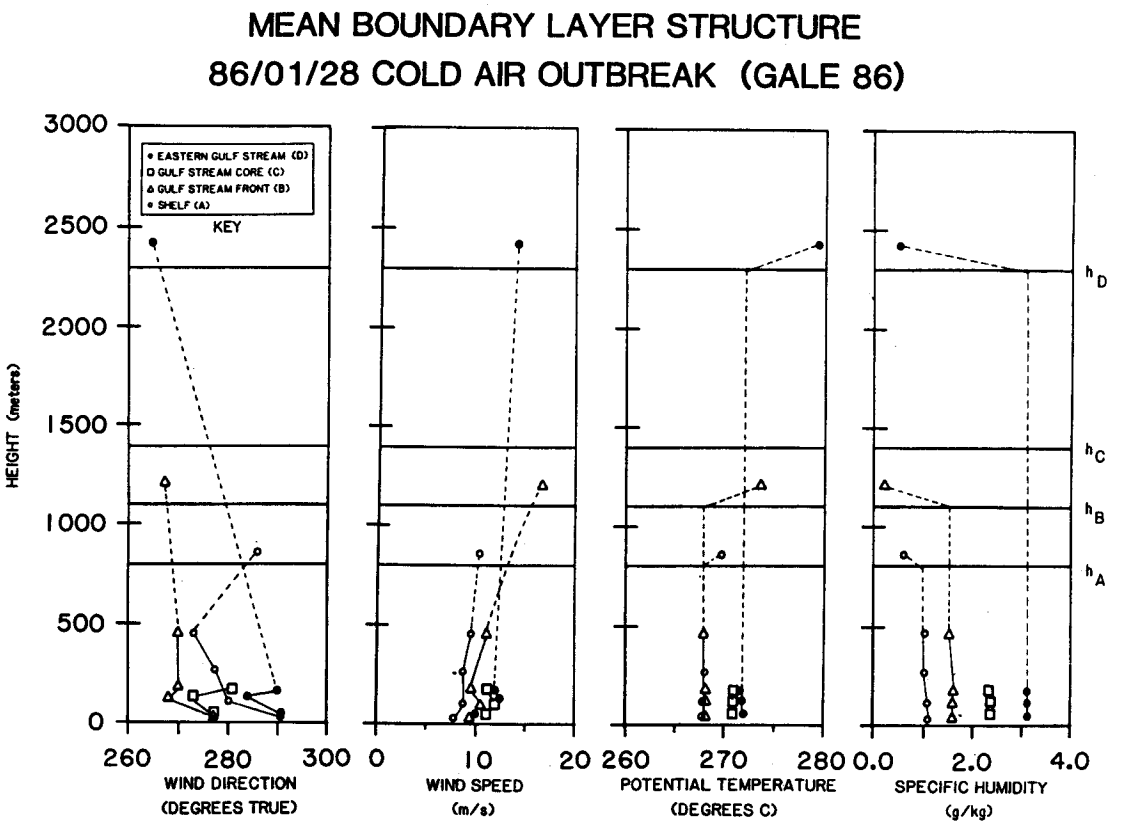

Fig. 7. Mean boundary-layer structure as measured by profiles of wind speed and direction, potential temperature and specific humidity. Dashed lines indicate regions where no crosswind flux data were collected.

These levels were predominantly in-cloud regions. Due to the highly convective, well-mixed nature of the MBL on 28 January, the profiles for temperature and humidity did not vary much within the sub-cloud region as expected. The profiles through the clouds are drawn as dashed lines because of the lack of data in that region.

The wind was observed to back between the lowest two levels at all four research locations, indicating the strong cold air advection near the surface. Also, the wind backed between the coast and point B, before veering again between points C and D. This initial turning of the wind could be in response to the decrease in surface roughness as the air moved from the land out over the water. The wind speed increased in the offshore direction, reaching its maximum near-surface value (11.1 m/s) over the core of the Gulf Stream (point C), and then decreased again towards the Sargasso Sea region. All the wind profiles show a jet-like feature at approximately 110 m, which coincides with a sharp change in wind direction.

The potential temperature profiles are plotted to allow easy detection of boundary layer height/depth. The profiles for all four areas display the charac-

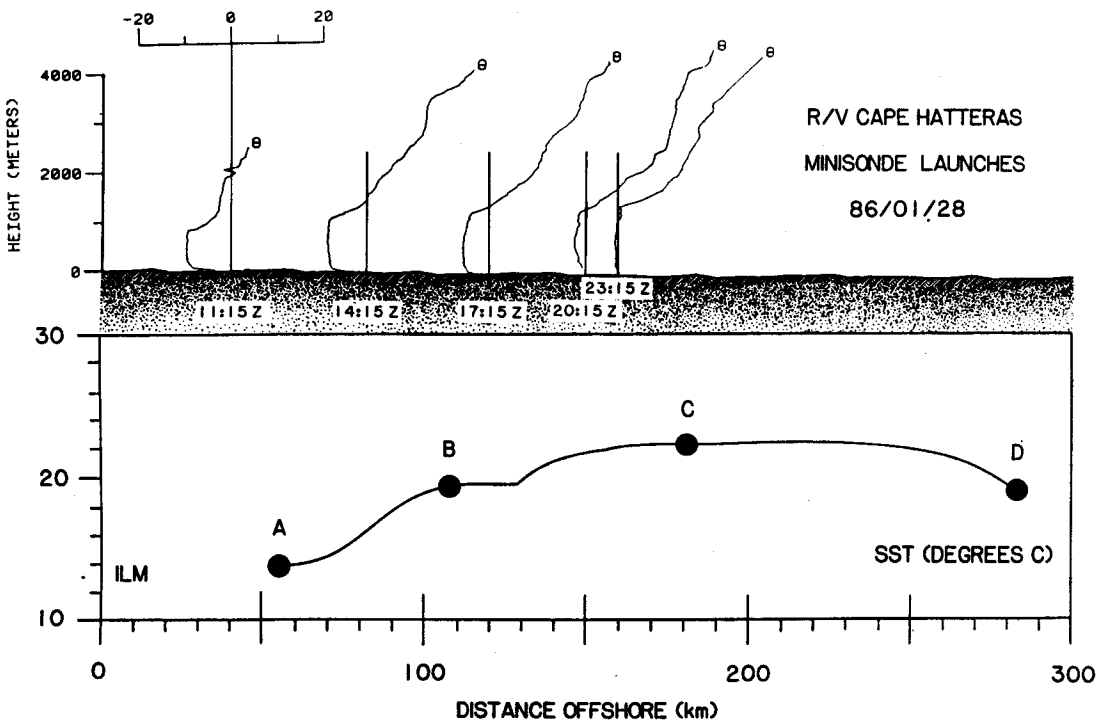

Fig. 8. Boundary-layer evolution and growth as depicted by the R/V Cape Hatteras minisonde launches. Data have been plotted with regard to the four aircraft research stations.

teristics of a well mixed, highly convective boundary layer growing in depth in the offshore direction. The growth in boundary-layer height is best observed by looking at Figure 8, which shows the potential temperature profiles from the 3-hourly minisonde launches on board the R/V Cape Hatteras. As noticed in the Electra profiles, the MBL offshore of Wilmington, North Carolina on 28 January, was warming and increasing in depth with distance offshore. The boundary layer height increased from 800 m at point A to 2300 m at point D, well east of the core of the Gulf Stream. All profiles showed a strong capping inversion. These results corroborate the earlier studies conducted by Chou *et al.* (1986) using the MASEX data, and SethuRaman *et al.* (1986) using ship and buoy data taken near the present study site offshore of the North Carolina coast.

The humidity profiles also showed the characteristics of a well-mixed, convective boundary layer. The humidity values were relatively constant below the inversion base, and then decreased quite rapidly above cloud top. This observation substantiated the results of the temperature profiles where the inversion base was found to correspond to the cloud tops rather than the cloud bases, a characteristic of tropical marine boundary layers where strong convection is present. The air mass modification could be observed in the humidity profiles as well, where the specific humidity increased from 1.09 g/kg at point A to 3.14 g/kg at point D.

Thus, the MBL was increasing in depth, warming and moistening in response

to the energy exchange processes between the cool air mass and the warmer underlying water. In addition, as has already been discussed in Figure 5, the thickness of the cloud layer increased along the trajectory taken by the aircraft and the cloud base decreased.

5.2. Turbulent Structure

In analyzing the turbulent structure of the MBL, only high-rate (or 20 sps) data were utilized. These data were used to generate statistical parameters representative of the turbulent properties of the area. Appropriate scaling parameters such as the surface friction velocity (u_*), the convective velocity scale (w_*), the convective temperature scale (θ_*), the convective humidity scale (q_*) and the Monin–Obukhov length (L) have been calculated as follows:

$$u_* = [(\overline{u'w'})_0^2 + (\overline{v'w'})_0^2]^{1/4}, \tag{1}$$

$$w_* = \left[\frac{g}{\theta_v} h(\overline{w'\theta_v'})_0\right]^{1/3}, \tag{2}$$

$$\theta_* = \left[\frac{(\overline{w'\theta_v'})_0}{w_*}\right], \tag{3}$$

$$q_* = \left[\frac{(\overline{w'q'})_0}{w_*}\right], \tag{4}$$

$$\mathrm{L} = -\left[\frac{\theta_v u_*^3}{kg(\overline{w'\theta_v'})_0}\right]. \tag{5}$$

In the above equations, h is the depth of the mixed layer, defined to be the height of the capping inversion, θ_v is the mean virtual potential temperature averaged along the lowest flight leg, k represents von Karman's constant (0.4), and g is the gravitational acceleration (9.81 m/s^2). The wind components are expressed in a positive east, north and upward coordinate system as u, v and w, respectively. All primed quantities denote turbulent statistics and the overbar indicates a mean value averaged over the length of the flight leg. The zero subscripts refer to values generated from data collected at the lowest flight level for each research station. Table II summarizes the above parameters for each research location sampled by the Electra.

Figure 9 shows the profiles of heat flux using the covariances of the fluctuations of humidity, potential temperature and virtual potential temperature. The values have been normalized by the lowest-level value. The altitudes for the lowest-level flux runs at each research station are given as follows: 38, 32, 49 and 48 m, respectively for stations A through D. The altitudes over the Gulf Stream and the eastern wall region of the Gulf Stream were higher because the sea surface was almost completely enshrouded by sea smoke. Further reduction in aircraft altitude in these regions would have made operations hazardous. The use of the

TABLE II

Boundary layer parameters for 28 January, 1986.

Research station	h (m)	$-L$ (m)	$-h/L$	u_* (m/s)	w_* (m/s)	θ_* (°K)	q_* (g/kg)
A	800	52	15	0.50	1.69	0.10	0.06
B	1100	93	12	0.74	2.30	0.13	0.09
C	1400	41	34	0.55	2.41	0.12	0.10
D	2300	29	81	0.40	2.31	0.07	0.07

lowest-level flight data for normalizing the flux profiles is considered valid, since the surface fluxes calculated from NCSU Buoy 2 (34° 12.0′ N, 77° 18.0′ W, Figure 2) using the iterative technique of Liu *et al.* (1979) were relatively close to the observed aircraft fluxes. The iterative technique was found to give reasonable values of surface turbulent fluxes for wind speeds up to 20 m/s (Akkarappuram and Raman, 1988), which is well above the aircraft-observed low-level wind speeds. Figure 10 shows the total (latent + sensible) heat flux and momentum flux calculated for Buoy 2. The Electra, using the eddy correlation technique, observed a total heat flux of 516 W/m^2 at 38 m, while the buoy measured a value of 500 W/m^2 at 10 m (for 2000 GMT) (Akkarappuram, 1988). Since currents in the vicinity of the Gulf Stream nominally approach 3–4 knots (1.5 to 2 m/s), moored buoys are almost impossible in this environment, and thus no surface flux comparisons were possible for stations B–D. However, based on the comparison at station A, the use of the lowest-level flight data for normalization of the flux profiles is deemed acceptable.

The heat flux profiles obtained using potential temperature and virtual potential temperature vary almost linearly with height and become negative at approximately $0.85h$. This result is in agreement with data collected for the monsoon boundary layer over the Arabian Sea (Holt and Raman, 1986a). In a similar study over the Bay of Bengal, the crossover occurred at $0.75h$ (Holt and Raman, 1986b). The reason for the negative flux near the inversion base is entrainment into the MBL from above. The humidity flux profiles also vary almost linearly with height, going to zero (or slightly negative values) around $1.10h$. After normalization by the lowest-level values, the flux profile values agree quite favorably in magnitude for the various regions studied.

When converted to proper units (W/m^2), the heat flux values give an indication of the amount of energy being transferred from the ocean to the amosphere. The sensible and latent heat transfer for 28 January increased substantially in the offshore direction, reaching its maximum value (1045 W/m^2) over the core of the Gulf Stream (point C). Although these values appear high, they are consistent with the strong winds and large air-sea temperature differences observed over the Gulf Stream. In response to these large fluxes, boundary layer height increased

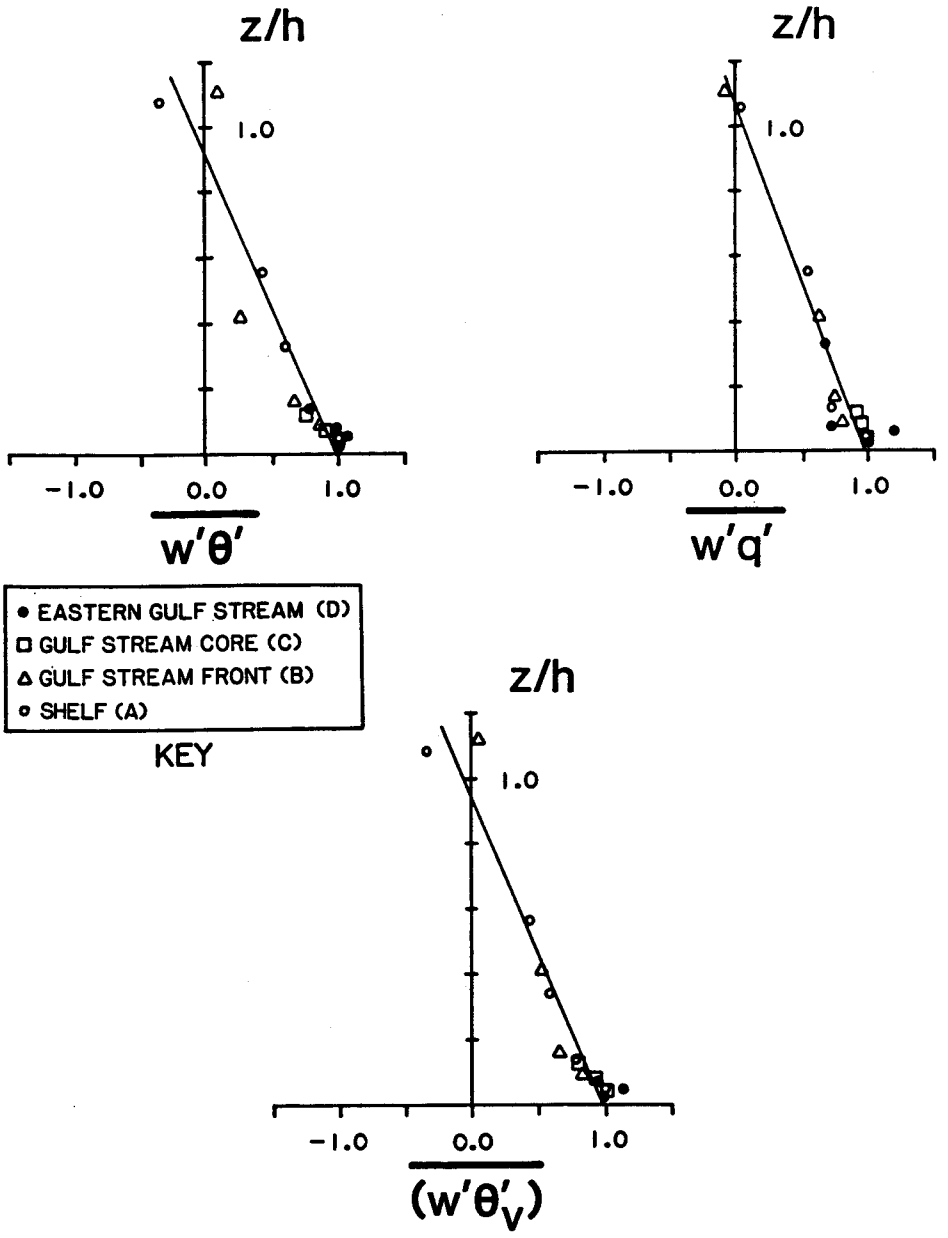

Fig. 9. Normalized temperature, humidity and potential temperature flux profiles. Each parameter has been normalized by the flux at the lowest flight level for each research station.

appreciably offshore (Figure 8). The observed MBL height of 1400 m at Station C was consistent with the calculated MBL height using the predictive equations of Venkatram (1977) and Gamo *et al.* (1983). The former method utilizes the land-water temperature difference and the offshore (downwind) distance, while the latter is based primarily on the total surface heat flux and the offshore

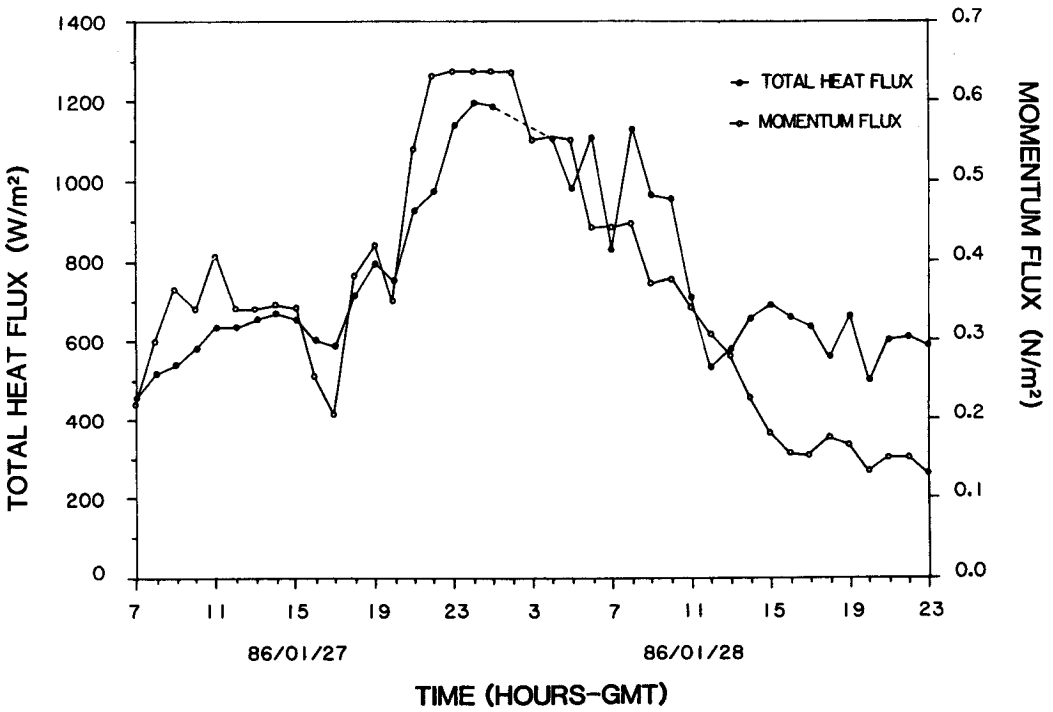

Fig. 10. Total (latent + sensible) heat flux and momentum flux for NCSU Buoy 2 for the period 86/01/27 0700 GMT to 86/01/28 2300 GMT, showing the response of the flux values to the intense cold air outbreak. The heat flux value at 86/01/28 2000 GMT was used in the aircraft comparison.

(downwind) distance. Both relationships employ the 1/2 power law for downwind boundary layer evolution/growth. Arya (1988) has cited the Gamo *et al.* method as the best equation for estimating boundary layer growth because its derivation involves the fewest assumptions.

When comparing the heat flux budgets with previous work, it would be beneficial to analyze the air-sea temperature difference prior to attempting interpretation. During this particular flight, the complexity of the underlying oceanic SST field has already been discussed. The aircraft encountered a mean SST gradient of 0.0679 °C/km over the flight path for station A (14.14 °C) to point C (22.56 °C), approximately a distance of 124 km. During MASEX (Chou *et al.*, 1986), SST variation was only 7 °C (5.5 to 12.5 °C) over the alongwind flight track, resulting in the largest SST gradient being 0.057 °C/km (along flight path AB, 80 km east-west) and the lowest gradient being 0.023 °C/km (along flight path BC, 100 km north-south). The sensible heat flux measurements on 28 January, 1986 are greater than those encountered during MASEX. When compared with the inner shelf values from this study, the MASEX data are only slightly (<50 W/m^2) less; however, when compared against the data collected over the Gulf Stream, the GALE flux values are almost twice those measured during MASEX. MASEX was conducted offshore of New Jersey and Delaware (35°–41° N, 76°–69° W) about 160 km north of the GALE region.

SethuRaman *et al.* (1986), using data collected in the region offshore of Cape Fear, North Carolina, encountered similar SST gradients (due to interaction with the Gulf Stream) but milder atmospheric conditions, with measured total (latent + sensible heat) flux values of about 600 W/m^2. The air-sea temperature difference during that study was only about 10 to 15 °C as opposed to approximately 24 °C for the present investigation. Also, Murty (1976) using AMTEX '75 results estimated total heat flux values in the Kuroshio region to be about 700–800 W/m^2. The maximum daily value reported in his analysis was 845 W/m^2, on 21 February, 1975, during an intense cold air outbreak over the Kuroshio current. Generally, the total flux values measured during AMTEX '74 were considerably lower than the AMTEX '75 results, due in part to much milder weather conditions.

Thus, the flux results are consistent with the previous observations although they are somewhat greater. The AMTEX data provide a good comparison with GALE due to the presence of warm western boundary currents in each study: Kuroshio and Gulf Stream, respectively. While MASEX was conducted over the mid-Atlantic shelf, it did not encounter the extremely warm currents of the Gulf Stream and thus the heat fluxes are considerably less than those measured on 28 January, 1986. Lowest level (38 m) values of heat flux from the aircraft compare well with the values obtained from the buoy by using the iteration technique (Akkarappuram and Raman, 1988).

In addition to the previously mentioned comparisons, this data set also provides the opportunity to investigate differences between the cloud-free (station A) and the cloud-capped (station B) MBL during highly convective conditions. For the cloud-free boundary layer (denoted by the open circles in Figure 9), the normalized total heat flux profile shows a positive maximum value at the lowest level (38 m), with an almost linear decrease throughout the MBL, reaching a negative maximum at the inversion level. These results compare quite favorably with the earlier findings of Sommeria and LeMone (1978), who analyzed turbulence data for the fair weather mixed layer near Puerto Rico.

Close examination of the heat flux data for station B (cumulus congestus/stratocumulus cloud-capped boundary layer, denoted by the open triangles in Figure 9), shows an almost linearly decreasing virtual potential temperature flux profile, ranging from a low-level maximum to approximately zero at the top of the cloud layer. This particular mission focused on the sub-cloud layer and thus no crosswind legs were flown in the cloud layer. However, a cloud-top run was completed to allow comparison of fluxes above the boundary layer. The moisture flux profile is very similar to the profile collected for the cloud-free boundary layer (station A), but with slightly negative values near the cloud top. This may be the result of the cloud top run intersecting the cloud layer at times during the approximately 8-min crosswind leg, due to the rapidly deepening MBL in this location. These findings do not agree with the results of earlier investigations of the stratocumulus-capped MBL (Brost *et al.*, 1982 and Albrecht *et al.*, 1985),

however; the discrepancies are probably due to the dominance of buoyancy over shear forces in the present case study. The presence of cumulus congestus and the large sensible and latent heat fluxes (these values are an order of magnitude larger for this GALE case study than the earlier stratocumulus experiment) are good indications of the highly convective conditions present in the region. In comparing the cloud-capped profile with the data collected during MASEX (Chou *et al.*, 1986), one finds good agreement. The scatter associated with the humidity data collected during MASEX is not found in the GALE data set, where the normalized moisture flux profile agrees quite well with a linearly decreasing curve. The better fit found in the GALE data is due possibly to the increased turbulent mixing experienced during this particular mission.

Figure 11 shows the standard deviations of the wind components, each normalized by the convective velocity scale (w_*). Two horizontal wind components show a near-equal contribution to the turbulence, decreasing with height from their near-surface maximum values. The relative high values near $z = h$ are probably due to the large wind shear near the top of the MBL. The vertical velocity component shows the characteristic maxima near 0.3 to $0.4h$, which have been observed by other investigators (Willis and Deardorff, 1974; Deardorff, 1980; Lenschow *et al.*, 1980). Once again, the failure of the sigma-w values to approach zero at $z = h$, is most likely due to the strong shear, entrainment and penetrative convection near the top of the boundary layer. Strong crosswind shear has also been associated with the generation of turbulence near the top of the MBL in MASEX (Chou *et al.*, 1986). The values for boundary-layer height and convective velocity scale at different offshore locations are given in Table II.

Using the assumption of stationary, the turbulent kinetic energy (TKE) budget can be expressed as follows:

$$0 = -\left[U\frac{\partial \bar{e}}{\partial x} + V\frac{\partial \bar{e}}{\partial y}\right] - \left[(\overline{u'w'})\frac{\partial U}{\partial z} + (\overline{v'w'})\frac{\partial V}{\partial z}\right]$$
$$+ \frac{g}{\theta_v}(\overline{w'\theta_v'}) - \left[\frac{\partial}{\partial z}(\overline{w'e'}) + \frac{\overline{(w'p')}}{\rho_0}\right] - \epsilon\,, \tag{6}$$

where the first terms on the right-hand side represent the alongwind and crosswind advection of TKE, respectively; the second bracketed terms are the alongwind and crosswind shear production, respectively; the third term is the buoyancy production; the fourth bracketed terms are the vertical transport of TKE and the pressure transport; and the last term is the viscous dissipation. The energy dissipation rate is estimated using the $-5/3$ inertial subrange law with the w-component winds using the following equation:

$$E_w(f) = a_w(\bar{u}_a/2\pi)^{2/3}\epsilon^{2/3}f^{-5/3}\,, \tag{7}$$

where f is the frequency, $E_w(f)$ is the vertical velocity spectra, a_w is the dissipation rate and $\bar{u}_a$ the speed of the aircraft. For the NCAR Electra crosswind

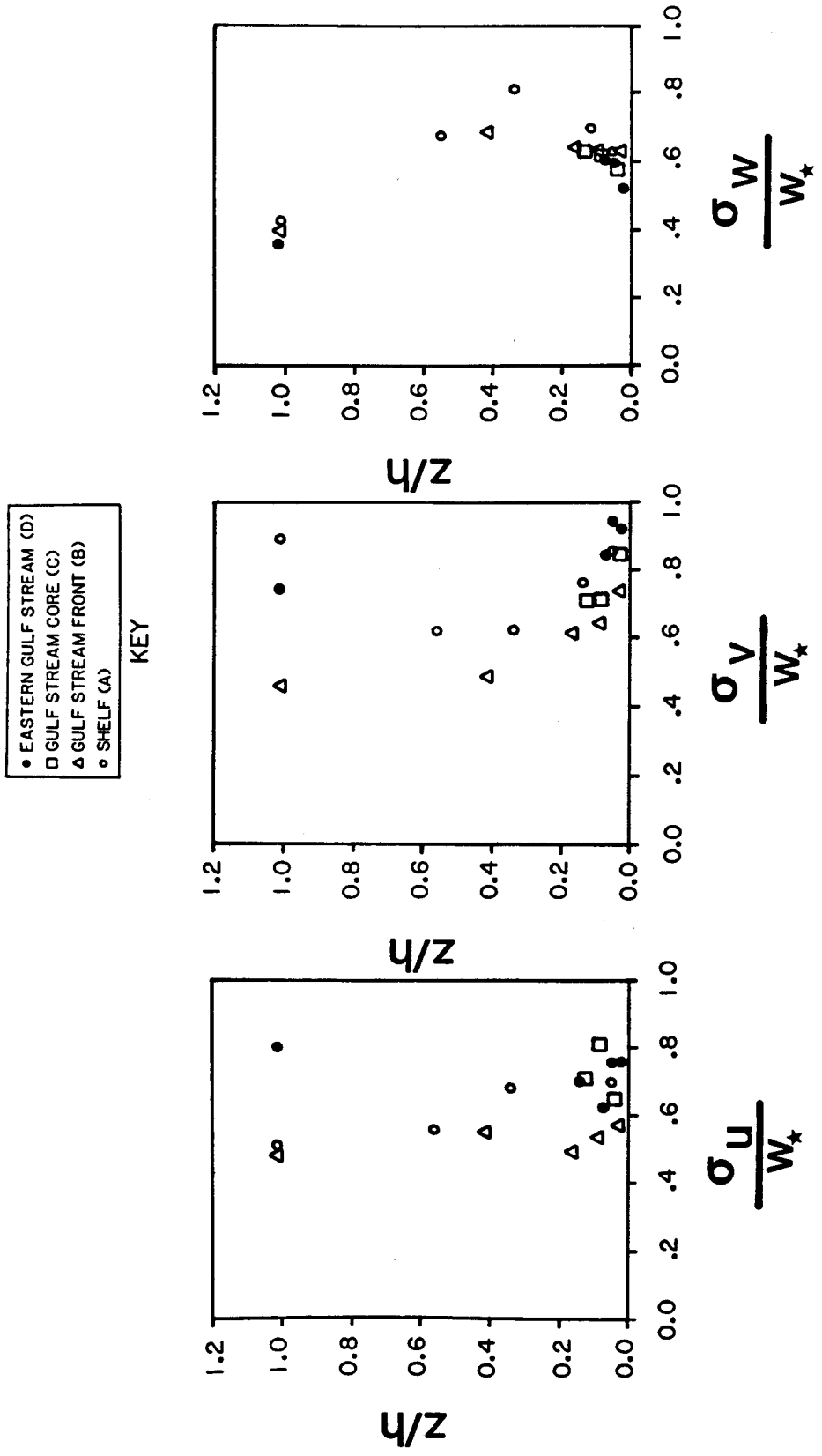

Fig. 11. Standard deviations of the velocity components normalized by the convective velocity scale (w_*) for each research location.

flight segments, u_a is approximately 100 m/s. a_w represents a constant and is equal to 0.67 for the vertical velocity component (Chou *et al.*, 1986). The pressure transport is considered to be a component of the residual term needed to balance the budget; however, there are other factors contributing to the total magnitude of this residual term (e.g., crosswind advection of TKE, sampling errors). The concept of horizontal homogeneity is valid in this case study as the computed values of the alongwind $(-U(\partial\bar{e}/\partial x))$ advection of TKE (10^{-5} to 10^{-4} m^2/s^3) are 2–3 orders of magnitude less than the other components (10^{-3} to 10^{-2}) in the budget. There is no means of accurately calculating the crosswind $(-V(\partial\bar{e}/\partial y))$ advection of TKE for this particular case study. However, it should be noted that the horizontal distance between crosswind legs appears to be the limiting variable in computing the alongwind advection of TKE (e.g., when using the finite-difference approximation for the partial derivative).

The turbulent kinetic energy budget, normalized by the lowest-level (A-38 m, B-32 m, C-49 m and D-48 m) buoyancy flux $((g/\theta_v)(w'\theta')_0)$, is presented in Figure 12. The budget represents all data collected at research stations A, B and C;

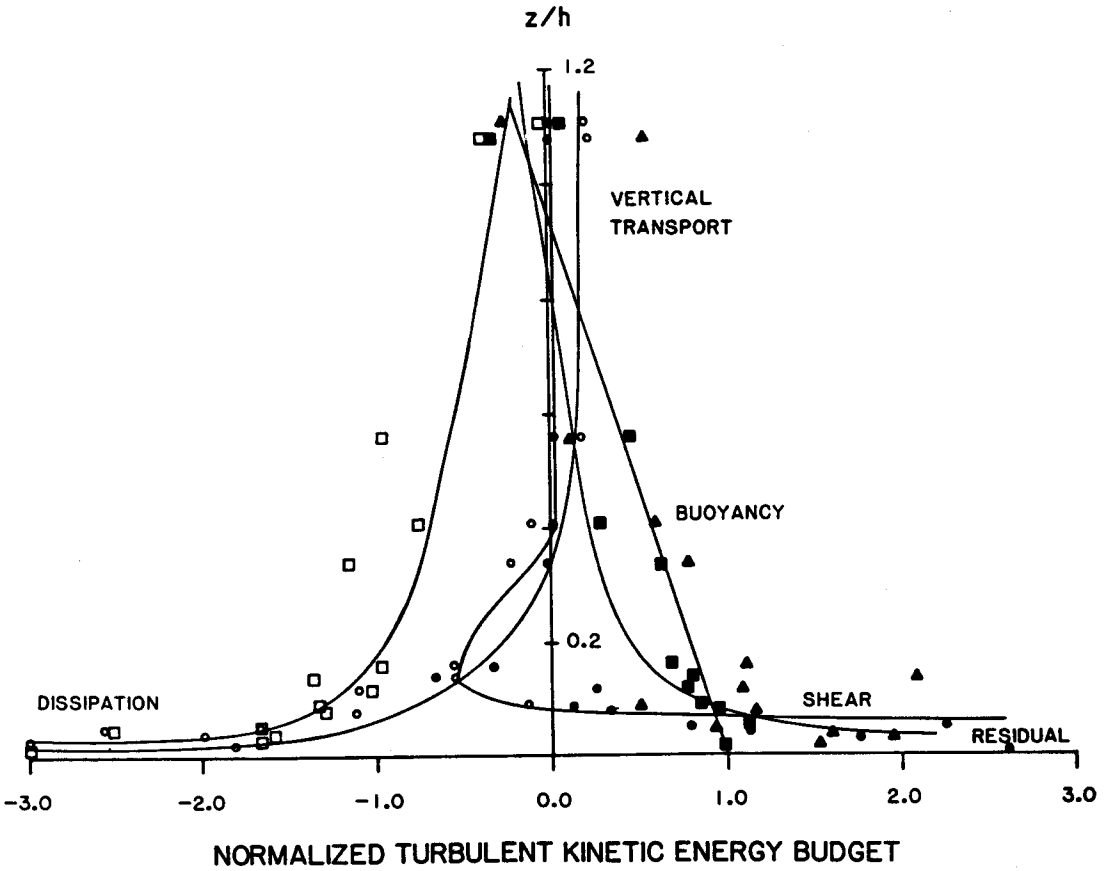

Fig. 12. Normalized turbulent kinetic energy (TKE) budget for crosswind research locations. Each value has been normalized by the buoyancy parameter for its respective location. Budget contains all data from locations A, B and C; however, only the lowest two levels from location D are included.

however, only the lowest two levels (48 m, 123 m) at location D have been included. The upper two levels at this latter location were omitted due to short sampling time and cloud interactions, respectively. Below $0.1h$, shear production was large after which buoyancy production dominated up to approximately $0.8h$ where shear once again became important along with the vertical transport of kinetic energy. Vertical transport of TKE is negative below $0.35h$, indicating a net loss of energy from these lower layers to the upper layers. This result is in good agreement with results from the marine monsoon boundary layer (Holt and Raman, 1986a,b) and earlier studies of the convective MBL (Lenschow *et al.*, 1980 and Chou *et al.*, 1986). Dissipation decreases monotonically with height, becoming almost negligible near $z = h$. The imbalance term, obtained as the residual of Equation 6, is a source term in the MBL below approximately $0.8z/h$, after which it serves as a small sink term in the budget. Comparison of the imbalance variation with the values for MASEX (Chou *et al.*, 1986) shows some similarity in shape; however, the crossover point ($0.8z/h$) of the curve is at a higher level in the GALE MBL than during MASEX, the major difference being the larger residual values at low-levels in the MBL during GALE. However, this is in agreement with the large shear production values measured at low levels during GALE as compared to the MASEX data. From this analysis it appears that one process that could reduce the low-level residual would be crosswind advection of TKE, which could not be accurately estimated from this particular data set.

Individual TKE budgets for research stations A (inner shelf) and B (shelf break) were computed and analyzed since they were flown over regions of markedly different surface conditions and contained data for the entire depth of the MBL (both above and below the inversion level). Figure 13 shows the non-normalized budgets of shear and buoyancy production for these two regions, plotted versus normalized height (z/h). Figure 13 shows the increased importance of shear at the lowest-levels of the MBL at station B, due to strong convergence at the western boundary of the Gulf Stream which resulted in increased winds speeds at this location. However, above approximately $0.1h$, the two locations appear to be relatively similar in terms of shear production. Huang and Raman (1988) have also found this low-level acceleration of the wind field in the vicinity of the Gulf Stream front using a two-dimensional, second-order closure MBL model. They attribute the process to the baroclinic effects found in the MBL during cold air outbreaks. Inspection of the buoyancy production term shows a strong increase in buoyancy forces over the warmer water at the shelf break location (B) as opposed to the cooler water on the inner shelf (A). The buoyancy profiles for the two areas begin to converge at approximately $0.4h$. Thus, buoyancy is important over a greater depth of the MBL than shear production, and the buoyancy production is increasing in the offshore direction, which is in good agreement with the previously discussed increase in MBL depth in this direction.

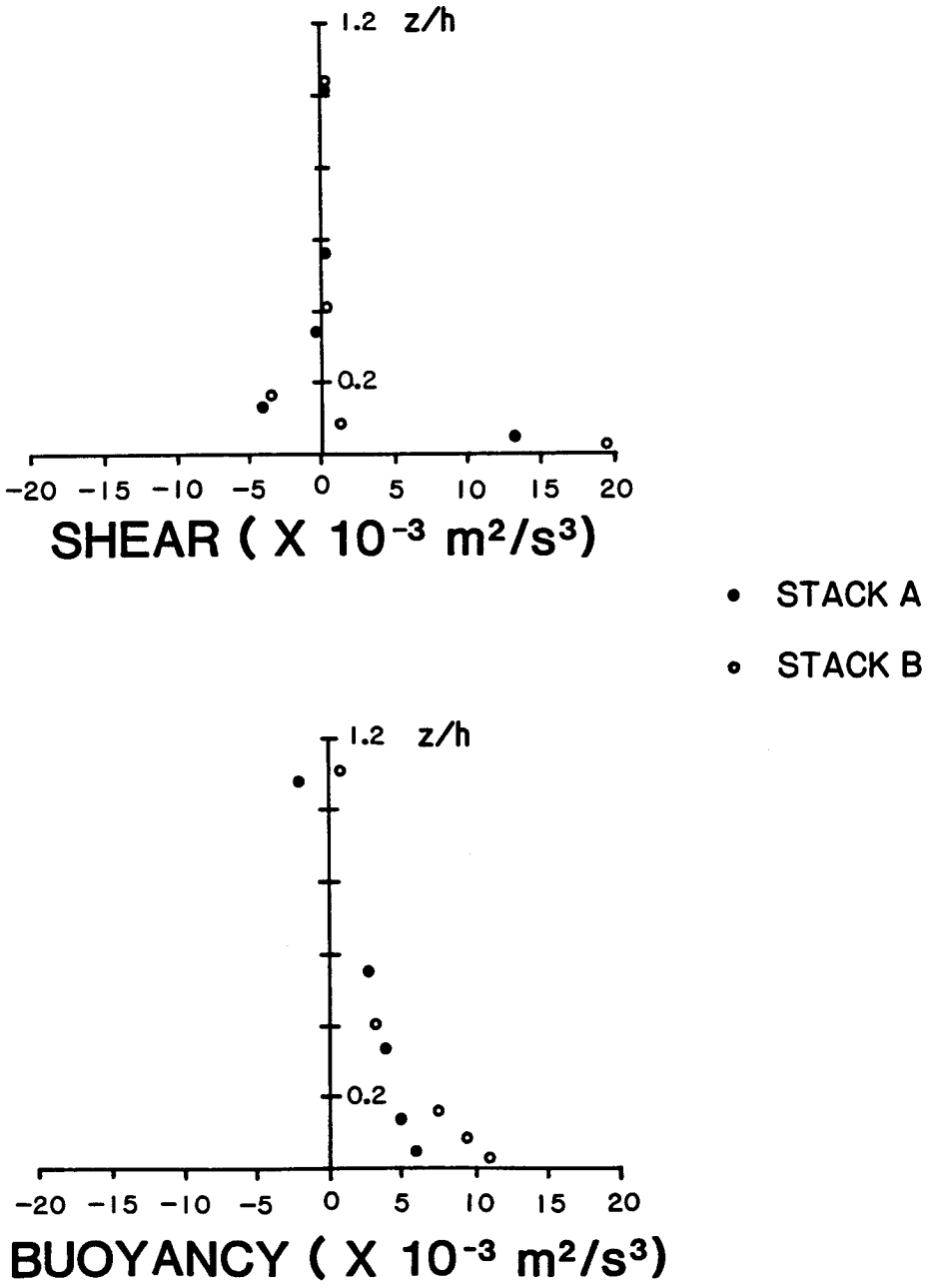

Fig. 13. Non-normalized shear and buoyancy profiles for research stations A and B, showing the increase in the low-level values at B as opposed to A.

In analyzing the non-normalized budgets of dissipation and turbulent transport (results not shown here), the same low-level dominance at B (as opposed to A) is found. Both terms are larger at station B than at A, below about $0.2h$. Above this level, dissipation and turbulent transport profiles behave similarly. The turbulent transport shows the crossover from sink to source (negative to positive) term near $0.5h$ at both locations. However, the increase in magnitude at B at lower levels is indicative of larger amounts of energy being transported from the lower layers of

the MBL to mid and upper layers as compared to station A. This finding also agrees favorably with the increase in MBL height with increasing distance offshore (downwind). The dissipation remains a sink term throughout the MBL depth, approaching zero at $z = h$ for bo locations. However, low-level values are greater at B than those observed at station A.

In comparison with the MASEX budget of Chou *et al.* (1986), one can find reasonably good agreement. The production side of the budget is dominated by buoyancy, while the destruction portion of the balance is predominantly dissipation. In addition, at low levels, shear ($<0.1\ z/h$) and turbulent transport ($<0.2 z/h$) are important source and sink terms in their respective budgets. The crossover of the turbulent transport (from sink to source term) occurs near $0.35h$, which agrees favorably with the total and individual TKE budgets presented here. The dominance of the shear term in the lowest levels of the GALE data could be attributed to the jet-like feature present in the wind profiles for each research station at the second lowest flight levels.

In comparison with the AMTEX budget of Lenschow *et al.* (1980), one finds a

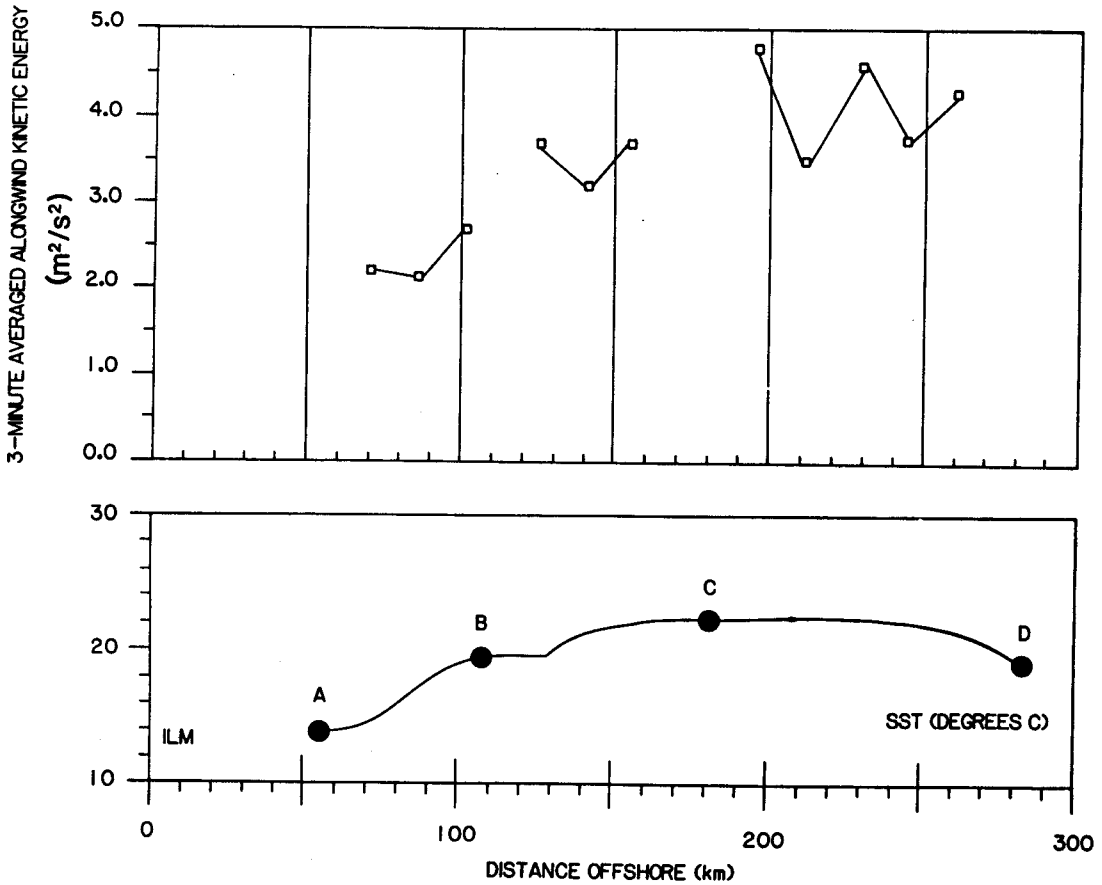

Fig. 14. Three-minute averaged alongwind kinetic energy (KE) measured during transit between research stations on the inbound phase of the aircraft mission. Measurements were made at approximately 41 m above sea level.

somewhat better agreement at the lower levels of the GALE MBL as compared to the MASEX (Chou *et al.*, 1986) TKE budget. Both buoyancy and dissipation dominate the respective sides of the budget; however, at the lowest levels shear does become the dominant source term. The turbulent transport term changes sign at approximately $0.375z/h$ and becomes the dominant source term above $0.8z/h$. Both of these findings agree favorably with the GALE and MASEX results. Thus, agreement between previous results and the GALE values is quite good. This also indicates the validity of similarity relations for highly convective boundary layers.

Due to changes in the properties of the air mass as it traverses the GALE region caused by the changing oceanic surface features, the TKE will also vary. Figure 14 is a time history of the turbulent kinetic energy ($\bar{e} = (\bar{u}'^2 + \bar{v}'^2 + \bar{w}'^2)$), computed from data collected along the lowest flight level during the inbound flight between research stations. The aircraft was travelling approximately into the mean wind during this time period. Each data point represents a 3-min (180 s or 3600 data points) average. The resulting figure, plotted with the underlying SST suggests an increase in TKE from stations D to C and then a decrease between stations C and A, as the aircraft moved over cooler water and a more thermally adjusted air mass. The alternating high-low values over the two offshore regions is indicative of mesoscale organized convection, similar to the Mesoscale Convective Cells (MCC) reported by Agee *et al.* (1973). The maximum value (4.79 m^2/s^2) in the time history occurs just prior to reaching station C and the lowest value (2.02 m^2/s^2) is on approach to station A. Thus, there is a significant variation of the turbulence in the baroclinic marine boundary layer caused by the sharp changes in the sea surface temperature field.

6. Summary and Conclusions

Aircraft, ship and satellite observations have been used to document the Marine Boundary Layer response to the 28 January, 1986 intense cold-air outbreak offshore of Wilmington, North Carolina. The air-mass modification processes caused the air to warm and moisten as it flowed out over the warmer coastal waters, the primary mechanism for this being the exchanges of latent and sensible heat between the ocean and the atmosphere. Near the Gulf Stream Core, a total heat flux of 1045 W/m^2 was measured at approximately 49 m above the ocean surface. The heat flux values decreased both landward and seaward of this maximum. These values were found to be larger than those measured in the MASEX and AMTEX '74 project and GALE values were comparable on only one day during AMTEX '75. The baroclinic effect was observed as a low-level (100 m) maximum in the vertical wind structure at all four offshore research locations.

In response to this increase in energy, the boundary layer height increased steadily in the offshore direction while cloud base decreased, effectively deepen-

ing the cloud layer. The deepening of the cloud layer resulted in the majority of the boundary layer being contained in the cloud region at the most offshore research station (D). When normalized by the low-level values, the flux profile values showed general agreement at different flight levels, indicative of similar contributing processes at each of the four crosswind stack regions.

In examining the turbulent structure, the two horizontal velocity components were found to contribute approximately equally to the turbulence, while the vertical component displayed the characteristic mid-boundary layer maxima. The TKE budget showed that buoyancy dominated the budget between 0.1 and $0.8h$, while shear became important above and below these levels. This result was also found in the AMTEX and MASEX budgets. Vertical turbulent transport was also found to be important above $0.8h$ as a source term, while it displayed a net transport of energy out of the layers below $0.35h$. Longitudinal advection of TKE was found to be insignificant for distances of the order of 100 km.

In general, the MBL on 28 January, 1986 was much more convective than in the AMTEX (Lenschow *et al.*, 1980), MASEX (Chou *et al.*, 1986) and pre-GALE (SethuRaman *et al.*, 1986) experiments. However, comparison between these data sets has shown reasonably good general agreement. This particular study has shown that the similarity relations are valid even under extremely convective conditions during an intense air mass modification event.

Acknowledgements

The authors would like to thank the University of Miami RSMAS for providing the software for analyzing the color satellite imagery; Dr Peter Hamilton (SAIC/Raleigh) for processing the images; Drs Larry Atkinson and John Bane for their help in obtaining the satellite data; Dr Robert Grossman (airborne mission scientist on 86/01/28) for his helpful discussions; and Ellen R. Wayland for typing the manuscript. This work was funded under National Science Foundation Grant #ATM-83-1182.

References

Agee, E. M., Chen, T. S., and Dowell, K. E.: 1973, 'A Review of Mesoscale Cellular Convection', *Bull. Amer. Meteorol. Soc.* **54**, 1004–1012.

Akkarappuram, A. F.: 1988, 'A Study of Air-Sea Exchange Processes off the Carolinas during the 1986 East Coast Winter Storms – GALE', Master's Thesis, North Carolina State University, Dept. Marine, Earth and Atmospheric Sciences.

Akkarappuram, A. F. and Raman, S.: 1988, 'A Comparison of Surface Friction Velocities Estimated by Dissipation and Iterative Bulk Aerodynamic Methods During GALE', *Geophys. Res. Let.* **15**, 401–404.

Albrecht, R. A., Penc, R. S., and Schubert, W. H.: 1985, 'An Observational Study of Cloud-Topped Mixed Layers', *J. Atmos. Sci.* **42**, 800–822.

Arya, S. P.: 1988, *Introduction to Micrometeorology*, Academic Press, Inc., San Diego, California, 307 pp.

Brost, R. A., Wyngaard, J. C., and Lenschow, D. H.: 1982, 'Marine Stratocumulus Layers. Part II: Turbulence Budgets', *J. Atmos. Sci.* **39**, 818–836.

Bunker, A. and Worthington, L. V.: 1976, 'Energy Exchange Charts of the North Atlantic Ocean', *Bull. Amer. Meteorol. Soc.* **57**, 450–467.

Chou, S.-H., Atlas, D., and Yeh, E.-N.: 1986, 'Turbulence in a Convective Marine Atmospheric Boundary Layer', *J. Atmos. Sci.* **43**, 547–564.

Chou, S.-H. and Atlas, D.: 1982, 'Satellite Estimates of Ocean-Air Heat Fluxes during Cold-Air Outbreaks', *Mon. Wea. Rev.* **110**, 1434–1450.

Colucci, S. J.: 1976, 'Cyclone Frequencies over the Eastern United States and Adjacent Western North Atlantic, 1964–1974', *Bull. Amer. Meteorol. Soc.* **57**, 548–553.

Deardorff, J. W.: 1980, 'Stratocumulus-Capped Mixed Layers Derived from a Three-Dimensional Model', *Boundary-Layer Meteorol.* **18**, 495–527.

Dirks, R. A., Kuettner, J. P., and Moore, J. A.: 1988, 'Genesis of Atlantic Lows Experiment (GALE): An Overview', *Bull. Amer. Meteorol. Soc.* **69**, 148–160.

Fernandez-Partegas, J. and Mooers, C. N. K.: 1975, 'A Subsynoptic Study of Winter Cold Fronts in Florida', *Mon. Wea. Rev.* **104**, 742–744.

Gamo, M., Yammamoto, S., Yokoyama, O., and Yoshikado, H.: 1983, 'Structure of the Free Convective Internal Boundary Layer above the Coastal Area', *J. Meteorol. Soc. Jpn.* **61**, 110–124.

Grossman, R. L.: 1988, 'Boundary Layer Warming by Condensation: Air-Sea Interaction during An Extreme Cold Air Outbreak from the Eastern Coast of the United States', preprint, Seventh Conference on Ocean-Atmosphere Interaction, Amer. Meteor. Soc., January 31–February 5, 1988, Anaheim, California.

Hayden, B. P.: 1981, 'Secular Variations in Atlantic Coast Extratropical Cyclones', *Mon. Wea. Rev.* **109**, 159–167.

Hayden, B. P. and Smith, W.: 1982, 'Season-to-Season Cyclone Frequency', *Mon. Wea. Rev.* **110**, 239–253.

Holt, T. and Raman, S.: 1986a, 'Variation of Turbulence in the Marine Boundary Layer over the Arabian Sea during Indian Southwest Monsoon (MONEX 79)', *Boundary-Layer Meteorol.* **37**, 71–87.

Holt, T. and Raman, S.: 1986b, 'Observations of the Mean and Turbulence Structure of the Marine Boundary Layer over the Bay of Bengal during MONEX 79', *Mon. Wea. Rev.* **114**, 2176–2190.

Huang, C.-Y. and Raman, S.: 1988, 'A Numerical Study of the Marine Boundary Layer over the Gulf Stream during Cold Air Advection', *Boundary-Layer Meteorol.* **45**, 251–290.

Huh, O. K., Rouse, L. J., and Walker, N. D.: 1984, 'Cold-Air Outbreaks over the Northwest Florida Continental Shelf: Heat Flux Processes and Hydrographic Changes', *J. Geophys. Res.* **89**, 717–726.

Lenschow, D. H. and Agee, E. M.: 1976, 'Preliminary Results from the Air-Mass Transformation Experiment (AMTEX)', *Bull. Amer. Meteorol. Soc.* **57**, 1346–1355.

Lenschow, D. H., Wyngaard, J. C., and Pennell, W. T.: 1980, 'Mean and Second-Moment Budgets in a Baroclinic, Convective Boundary Layer', *J. Atmos. Sci.* **37**, 1313–1326.

Liu, W. T., Katsaros, K. B., and Businger, J. A.: 1979, 'Bulk Parameterization of Air-Sea Exchanges of Heat and Water Vapor Including the Molecular Constraints at the Interface', *J. Atmos. Sci.* **36**, 1722–1735.

Mercer, T. J. and Kreitzberg, C. W.: 1986, 'GALE Field Program Summary', GALE Data Center (GDC), Drexel University, Philadelphia, Pa., 447 pp.

Miller, E. R. and Friesen, R. B.: 1985, 'Standard Output Data Products from the NCAR Research Aviation Facility', NCAR RAF Technical Bulletin No. 9, 64 pp.

Murty, L. K.: 1976, 'Heat and Moisture Budgets over AMTEX Area during AMTEX '75', *J. Meteorol. Soc. Jpn.* **54**, 370–381.

Nowlin, W. D. and Parker, C. A.: 1974, 'Effects of a Cold-Air Outbreak on Shelf Waters of the Gulf of Mexico', *J. Phys. Ocean.* **4**, 467–486.

Raman, S. and Riordan, A. J.: 1988, 'The Genesis of Atlantic Lows Experiment: The Planetary Boundary Layer Subprogram', *Bull. Amer. Meteorol. Soc.* **69**, 161–172.

Sethu Raman, S., Riordan, A. J., Holt, T., Stunder, M., and Hinman, J.: 1986, 'Observations of the Marine Boundary Layer Thermal Structure over the Gulf Stream during a Cold-Air Outbreak', *J. Appl. Clim. Meteorol.* **25**, 14–21.

Sommeria, G. and LeMone, M. A.: 1978, 'Direct Testing of a Three-Dimensional Model of the Planetary Boundary Layer Against Experimental Data', *J. Atmos. Sci.* **35**, 25–39.

Uccellini, L. W., Brill, K. F., Petersen, R. A., Keyser, D., Aune, R., Kocin, P. J., and des Jardins, M.: 1986, 'A Report on the Upper Level Wind Conditions Preceding and during the Shuttle Challenger (STS 51L) Explosion', *Bull. Amer. Meteorol. Soc.* **67**, 1248–1265.

Venkatram, A.: 1977, 'A Model of Internal Boundary Layer Development', *Boundary-Layer Meteorol.* **11**, 419–437.

Willis, G. E. and Deardorff, J. W.: 1974, 'A Laboratory Model of the Unstable Planetary Boundary Layer', *J. Atmos. Sci.* **31**, 1297–1307.